American Mineralogist, Volume 98, pages 1449–1458, 2013

Mechanical spectroscopy in twinned minerals: Simulation of resonance patterns at high frequencies† 🔓

Ekhard K.H. Salje,[1,2,*] Ziyuan Zhao,[2] Xiangdong Ding,[2] and Jun Sun[2]

[1]Department of Earth Sciences, University of Cambridge, Cambridge CB2 3EQ, U.K.
[2]State Key Laboratory for Mechanical Behavior of Materials, Xi'an Jiaotong University, Xi'an 710049, China

Abstract

Computer molecular dynamics (MD) simulations of dynamically driven twin structures reveal the main results of resonance ultrasonic spectroscopy (RUS) and dynamic mechanical analysis (DMA), namely the high-friction damping at low frequencies, and underdamped oscillations at high frequencies. High-frequency spectra show absorption, which relates to phonon heating of the sample and phase shifts between the applied dynamical strain field and the geometrical movements inside the microstructure. Two main excitations have been identified to describe this behavior. The first is the progression and retraction of needle twins, the second is the movement of kinks inside twin boundaries. The dynamical response of these excitations has been simulated over large frequency and amplitude regions. It is shown that propagations of needle twins and kinks have a propensity to irreversibility when needles completely retract and destroy themselves and when kinks disappear at the sample surface. These movements lead to macroscopic "jerks" or spikes in the heat content of the sample. At higher frequencies, all movements become oscillatory with very small amplitudes, which, below a cut-off of one lattice unit, are simple phonon vibrations. These movements are continuous and do not contribute to the jerk-spectra. The connection between the simulated microstructures and the dynamical elastic measurements are discussed.

Keywords: Mechanical properties, dynamical mechanical analyzer, resonant ultrasonic spectroscopy, ferroelastic, twin, microstructure, needle domains, ferroelastic kinks

Introduction

Mechanical properties of minerals have been analyzed for many decades with emphasis on single crystals (e.g., Haussuehl 1960). With the advent of (multi) ferroic materials in physics and material sciences, the same techniques, such as low-frequency DMA measurements and high-frequency resonant ultrasonic spectroscopy (RUS) have been used to characterize mechanical properties and yield significant advances in both experimental techniques and the interpretation of mechanical spectra (Salje and Schranz 2011; Carpenter and Salje 1998; Scott et al. 2012). Recent work in the mineralogical literature such as Zhang et al. (2012a, 2012b), Prencipe et al. (2009), Harrison et al. (2003, 2004a, 2004b), Ohno et al. (2000), Isaak and Ohno (2003), Isaak et al. (2006), McKnight et al. (2007), Carpenter et al. (2007), and Salje et al. (2011a, 2011b, 2011c) use DMA and RUS methods to determine the temperature and pressure dependence of elastic moduli to understand by which mechanisms phase transitions in minerals occur. All ferroelastic phase transitions show strong temperature and pressure dependencies of the elastic moduli near the transition points [for a review Carpenter and Salje (1998) and Salje (2012)].

The theoretical analysis of experimental DMA and RUS spectra uses two different approaches. The first follows the initial treatment of elasticity by Born and Huang (1954) where the uniform deformation is replaced by the "long wavelength" approximation in wave vector space and the implicit assumption that most displacements can be understood using the full spectrum of wave vectors as was developed later in the work by Khatchaturyan and his collaborators (e.g., Kachaturynan 2008). The macroscopic elasticity is then evaluated as space averaged, i.e., the stress and the strain are summed up to macroscopic quantities with an "effective" elastic tensor as proportionality factor between them. This idea is covered by the effective medium theories such as the Hashin Shtrikman theory (Hashin and Shtrikman 1963); similar approaches are compiled in the extensive work of Milton (2002). The effective medium analysis is widely used in material sciences where the macroscopic performance of materials is relevant. It is also used in seismology. Seismic waves have very long wavelengths and—at least in the far field—small amplitudes so that an effective medium approach appears to be the appropriate approximation (Ben-Zion and Lyakhovsky 2002; Jackson et al. 2009; Baró et al. 2013). It should be noted, however, that even in this case the effect of interfaces and atomic diffusion related to the movement of interfaces is important and leads sometimes to significant modifications of the effective elastic moduli (Jackson et al. 2006; Salje 2007, 2008). For glasses, see the papers by Samwer and collaborators (e.g., Schroder et al. 1985).

An alternative approach is taken in this work. We focus on microstructures and consider dynamic excitations. In ferroelastic

* E-mail: ekhard@esc.cam.ac.uk

† 🔓 Open access: Article available to all readers via GSW (http://ammin.geoscienceworld.org) and the MSA web site.

materials, the complex microstructures consist of interpenetrating twin boundaries, and it is often not possible to predict the excitation spectra of such complex patterns. Two types of observations exist for moving interfaces. When the interface relaxes under the applied strain in a continuous fashion, one observes reduced elastic moduli, elastic absorption, and changes of phase angles. The second feature, which has not been explored systematically in minerals, are the emission of short signals related to rapid events, such as pinning and unpinning of interfaces, the formation of cracks, etc. These effects are collectively known as "jerks" and have been investigated for almost 100 years in magnets as Barkhausen jumps or avalanches (Spasojevic et al. 1996; Mehta et al. 2002; Sethna et al. 2001; Ding et al. 2012; Salje et al. 2011a, 2012). Their origin stems from the complexity of the domain patterns, the randomness of defects distributions, etc. Only in simple patterns are elastic responses related to the dynamical behavior of individual twin boundaries (Salje 2008, 2012; Salje and Zhang 2009a, 2009b) and will only in cases of extremely strong pinning mirror the intrinsic elastic moduli of the matrix or the composite of a matrix with finely dispersed interfaces (Goncalves-Ferreira et al. 2009; Salje et al. 2009; Lee et al. 2006; Calleja et al. 2003). Fast events related to the movement of domain boundaries are often superposed by slow events at larger forces, such as grain boundary sliding motions (review Morris and Jackson 2009). These events are not considered in this study.

The importance of this second approach is not so much the determination of elastic moduli but lies in the analysis of energy dissipation and the mechanism of "jerky" and smooth relaxations of domain patterns as discussed in detail by Gallardo et al. (2010) and Salje et al. (2011b, 2011c). The movement of twin boundaries, as the most common microstructure in such studies, was analyzed in detail by Schranz et al. (2009), Salje and Zhang (2009b), Daraktchiev et al. (2007), and Harrison et al. (2004a, 2004b). Jerky behavior is very common in minerals and only in extremely pure crystals is the pinning of domain wall movement too weak to be observed. An example is high-purity $SrTiO_3$ (Kityk et al. 2000) where internal structural changes of the domain walls themselves can still lead to changes of RUS spectra (Scott et al. 2012). This approach also allows us to determine intrinsic ferroic properties of twin boundaries, which form the base for the emerging field of twin boundary engineering (Salje 2010; Van Aert et al. 2012). Jerks have been also observed when minerals undergo stepwise phase transitions with the nucleation of complex microstructures and the collapse of porous media (such as SiO_2, goethite, and Al_2O_3) under stress (Salje et al. 2009, 2011a, 2011b, 2011c, 2013; Romero et al. 2011; Vives et al. 2011; Perez-Reche et al. 2004; Vives and Planes 1994).

The propagation of twin boundaries and interfacial boundaries under external stress is "overdamped" at low frequencies, i.e., the analysis is in the limit where the accelerating forces at the interfacial front are ignored while the momentum forces are identified as the driving forces. The physical effects relate to the emission of phonons or pinning/unpinning effects of the interface so that—after time averaging—local acceleration is replaced by a constant speed movement. Collective motions of domain walls DMA experiments are in this category and have been observed optically (Harrison et al. 2004). For low temperatures and small forces, it was found that the anelastic response is dominated by advancement or retraction of combs of needle domains. At higher temperatures, lateral translation of twin walls also contributes to the response. Cole-Cole plots of the response at small forces show depressed semicircles, which are well described by the Cole-Cole equation of a Debye peak with a broadening exponent μ

$$J(\omega) = J_u \Delta J/(1 + i\omega\tau_o)^{\mu}.$$

Physically, this model corresponds to a Debye-like relaxation process with a distribution of relaxation times around τ_o. The shape of the distribution and its width are described by the exponent μ [$0 < \mu \leq 1$, see Salje and Schranz (2011), for a review].

In high-frequency RUS experiments, one observes domain movements, which are characterized by 4 parameters, namely the resonance frequency ω_i, the amplitude A_i, the damping Q, and the phase shift φ (e.g., Migliori and Maynard 2005). RUS signals are not local resonances but represent the vibration of the entire sample and the attached RUS equipment (sample rods and transducers). In an RUS experiment, the driving transducer leads to sustained vibrations of the sample (the "ringing" of the sample), with an amplitude, which is detected by the receiver transducer. The complex amplitude is given by a sum of oscillators (or some other combination reflecting the effective medium of the sample)

$$x(\omega,t) = \Sigma\{A_i A_{excitation}/[\omega_i^2 - \omega^2 + i\omega_i\omega/Q]\} \exp(-i\omega t + \varphi),$$

$A_{excitation}$ is the amplitude of the forcing field, normally the strain or the stress, which is applied to the sample. The complex amplitude can be split into the real part $R(\omega)$ and the imaginary part $I(\omega)$. Their trajectories, $I(\omega)$ vs. $R(\omega)$, can be displayed as Cole-Cole plots (or Nyquist plots) (Kremer and Schonhals 2002; Lee et al. 2004) whereby each (underdamped) resonance becomes a circle through the origin. This circle is rotated by the phase φ around the origin. When the control parameter is changed, resonances and excitations in the RUS frequency range may change the phase factor. The fundamental challenge for the interpretation of RUS spectra is to understand the meaning of the phase shift φ, which does not exist in the overdamped DMA experiments. One expects no change of the RUS phase φ if a sample has a stable microstructure, which does not depend on the control parameter. This is born out in quartz where RUS phase angles are virtually independent of temperature (Lee et al. 2004). In $BaTiO_3$ one finds the same situation in the orthorhombic phase where the microstructure is frozen but not in the tetragonal phase where the microstructure can be excited dynamically. The phase angle changes near the phase transition in $LaAlO_3$ but not at lower temperatures (Salje and Carpenter 2011). The geometrical movement of needle domains in RUS experiments is much smaller than in DMA experiments: if we assume that the speed of the movement to be the same, then we will have typically needle domains moving by some six orders of magnitude less than in DMA settings. The observed movement (Harrison et al. 2004) is ca. 5 mm so that the RUS movement would be some 0.5 nm. This corresponds to some few unit cells of a typical crystal structure. We focus on this length scale in

our simulations (0–20 unit lengths). RUS displacements are hence truly on an atomic level and that is why we simulate their movements by molecular dynamics (MD) techniques rather than using continuums mechanics.

The key missing link between the analysis of RUS spectra and the physical interpretation of changing domain patterns is a clear understanding of the origin of the damping and the phase angle by simple twin wall movements. To fill this gap we have undertaken extensive MD simulations of various twin patterns under external strain and have found that only two fundamental excitations suffice as the origin of the observed parameters, namely retracting and advancing needle domains, and mobile kinks in domain walls. These are also the origin of the jerks when they break loose from pinning centers. It is the purpose of this paper to report the results of our simulations and to emphasize the close relation between phase changes in RUS, pinning behavior and jerks.

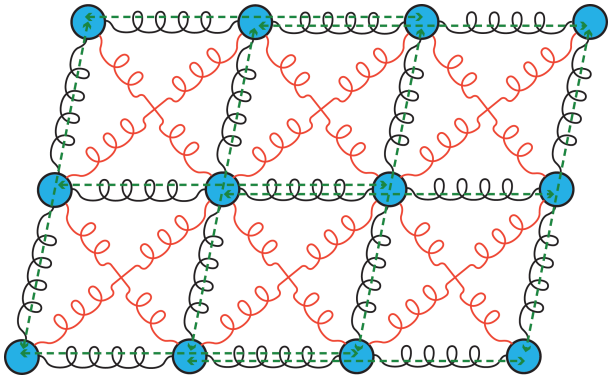

FIGURE 1. The model with nearest-neighbor (black springs), next-nearest-neighbor (red springs), and third-nearest-neighbor (green lines) interactions.

THE MODEL

We simulate a ferroelastic material using the initial ideas of Salje et al. (2011a). Our model is based on interatomic interactions (Ding et al. 2006; Deng et al. 2010) rather than coarse-grained simulations (Groger et al. 2008) because the elementary step leading to advancing twin boundaries is known to involve the sideways movement of kinks inside these boundaries (Salje et al. 1987; Froseth et al. 2004). Such atomic scale kinks are well reproduced by atomic scale simulations, whereas coarse-grained methods average over such fine structural details (Boussinot et al. 2010). The interatomic potentials were chosen to reproduce most closely the mesoscopic Landau potentials of the relevant materials (Jacobs 2000; Salje and Parlinski 1991; Salje 2010). As the shear angle of ferroelastic materials (Parlinski et al. 1993) is typically below 4° compared to many martensitic materials that often have larger shear angles, we constructed the model so that the shear angle was fixed to 4°, a good compromise for metallic as well as oxide materials. The simulations were conducted with three interactions in a monoatomic, two-dimensional lattice (Salje et al. 2011a). The potential contains harmonic springs along the sides of the sheared unit cell (nearest neighbors, Vnn), Landau springs in the diagonal (next nearest neighbors, Vnnn) and fourth-order interactions (springs) between the third nearest neighbors (Vnnnn). The resulting potential is a sum of the three interactions

$V(r) = V_{nn}+V_{nnn}+V_{nnnn}$ with $Vnn = 20(r - 1)^2$ (black springs in Fig. 1)

$Vnnn = -10(r - \sqrt{2})^2 + 2000(r - \sqrt{2})^4$ (red springs online in Fig. 1)

$Vnnnn = -(r - 2)^4$ (long dashed green lines in Fig. 1)

where r is the distance vector.

The initial conditions contain sandwich configurations with two buffer layers on the top and bottom of the two-dimensional sheet. The system was then relaxed using a conjugate gradient refinement procedure to find the optimal position for each lattice point and a modified shear angle. Molecular dynamics was then performed to anneal each configuration at a given temperature for 10^6 time steps. After this relaxation, prescribed shear strain was applied at the upper and lower buffer layers of the sample, which stabilizes one domain orientation (+4°) and destabilizes the other (–4°). Free boundary conditions are used because domain boundaries have been observed to nucleate as needle domains from the crystal surface.

Previous works (Salje et al. 2011a; Ding et al. 2012), showed that increasing strain on the upper and lower buffer layers is initially compensated by an elastic deformation until a threshold is reached where the unstable domain decomposes usually into a multitude of twinned micro-domains. The emerging twin patterns are usually very complex and contain most of the important dynamical features moving needle domains and kinks. The present work focuses on these two fundamental excitations (the movement of needle domains and kinks) at different frequency of dynamical load. They are, first, a needle domain under an oscillatory strain (Fig. 2a), and second, an excitation and movement of kinks (or latches) inside domain walls (Fig. 2b) under an oscillatory strain.

Unlike Salje et al. (2011a) where the shear strain increased linearly with time, here we choose an oscillatory time dependence for the shear strain $e = e_o + \Delta e$, where $\Delta e = A \sin(\omega t)$, which mimics the frequency dependence of RUS experiments. For the movement of the needle domain, we set the external strain e_o to the de-pinning point where the needle just detaches itself from the horizontal twin boundary in Figure 2a. For the movement of kinks, e_o corresponds to zero stress, so that the strain oscillation is symmetric with respect to the zero stress. The temperature for the simulation of a kink movement was set to be 0.1 T_{VF}. Here and elsewhere, T_{VF} refers to the Vogel-Fulcher temperature. This temperature limits the thermally excited kink movement to the athermal regime. Thus our simulations on kinks are essentially athermal so that thermal excitations are irrelevant for the analysis. The corresponding statistical collective behavior of a twin pattern at this temperature is described by a power law probability P(J) of pinning and unpinning events J: $P(J) \sim J^{-\epsilon}$ (Salje et al. 2011a). The temperature of the simulations of needle domains was T_{VF}.

The molecular dynamics code used in the present calculations is LAMMPS. NVT ensembles were used for the movement of needle domains and kinks, except the NVE ensemble was also adopted when analyzing the friction heating of both needle

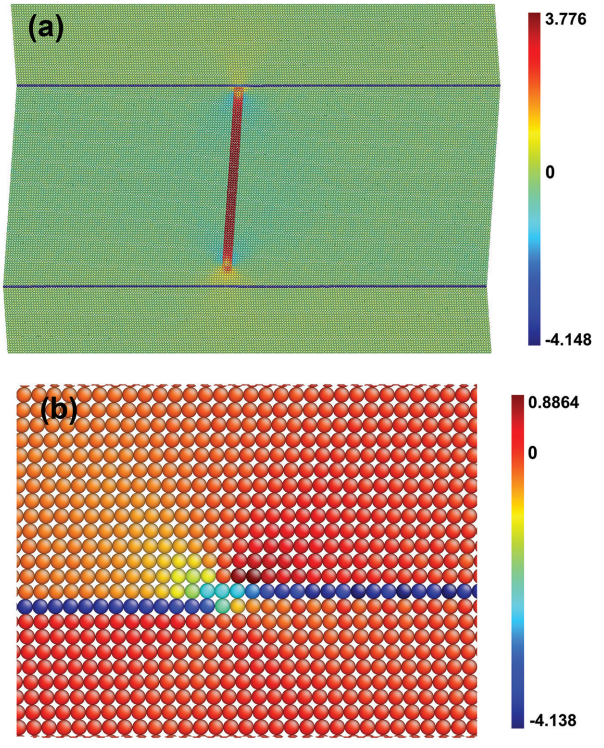

FIGURE 2. Sheared unit cell of the driven systems introduces microstructures, which consist in the most simple case of needle domains and kinks in twin walls. (**a**) The single needle domain (red) connects the two horizontal twin boundaries (blue) at the initial stage and then retracts from the lower twin boundary. (**b**) The kink is equally driven by external strain. Note the lattice deformation near the kink position. The colors indicate the local shear angle in the plane ($\alpha_{horizontal} + |\alpha_{vertical}| - 4°$). The drag of this deformation sets the timescale for the "free" kink movement, which is lower than the phonon time.

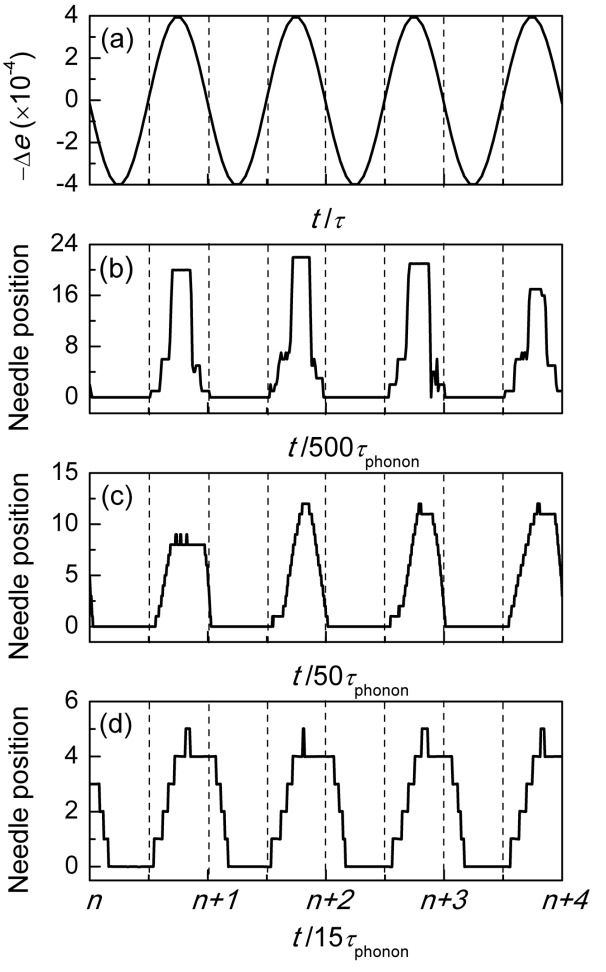

FIGURE 3. Position of the needle tip compared with the driving strain oscillation [$\Delta e = A \sin(\omega t)$]. τ is the time period of input sine-wave and τ_{phonon} is the time period of phonons. (**a**) shows the change of Δe with time, (**b**–**d**) shows the change of needle position under different time period of input sine-wave Δe, in which the time period is 500 τ_{phonon} in **b**, 50 τ_{phonon} in **c**, and 15 τ_{phonon} in **d**. Note the increasing width of the profile when the frequency is increased. The onset of the domain retraction is retarded with respect to the reflection points of the driving force while the progression of the needle starts later than the reversed oscillatory driving strain (Δe). The profiles are non-symmetric with slow retraction and faster progression.

movement and kink movement. We note that, the timescale of the intrinsic "phonon" movement of this model is given by its mechanical nature: the harmonic and anharmonic springs mimic the mechanical deformation of the structure on timescales, which follow from the dissipation-fluctuation theorem. The timescale of thermal fluctuations is then also the timescale of the susceptibility and hence of the mechanical resonance. We use the term "phonon time" in the sense that this mechanical response sets the frequency scale of the simulation.

RESULTS

Needle domains

We first describe the movement of needle domains. In Figure 3 we show the dynamical movement of a needle tip when the macroscopic strain is changed harmonically. The shift of the response function, namely the position of the needle tip as function of time, implies an increase of the phase angle φ. With decreasing strain the needle first unpins from the orthogonal wall (Fig. 2a) before it starts its upward movement. This movement continues for a short time interval even when the driving strain increases. Renewed pinning occurs when the needle hits the horizontal wall, which is not at zero relative strain Δe but, at higher frequencies, only when Δe is reversed (Fig. 3). The overall time evolution of the tip position is again a periodic (but not harmonic) function and contains a phase shift, which increases with increasing frequency.

Figure 4 shows the Lissajous curves for 3 characteristic frequencies. At low frequencies, the strain and needle position move almost in phase. With increasing frequency we find the phase angle to change toward $\pi/2$ where the Lissajous curve becomes a circle. The phase shift with frequency (or any other control parameter) is hence due to the retardation of the needle movement with respect to the exciting strain field. The corresponding Nyquist plots are then rotated circles through the origin,

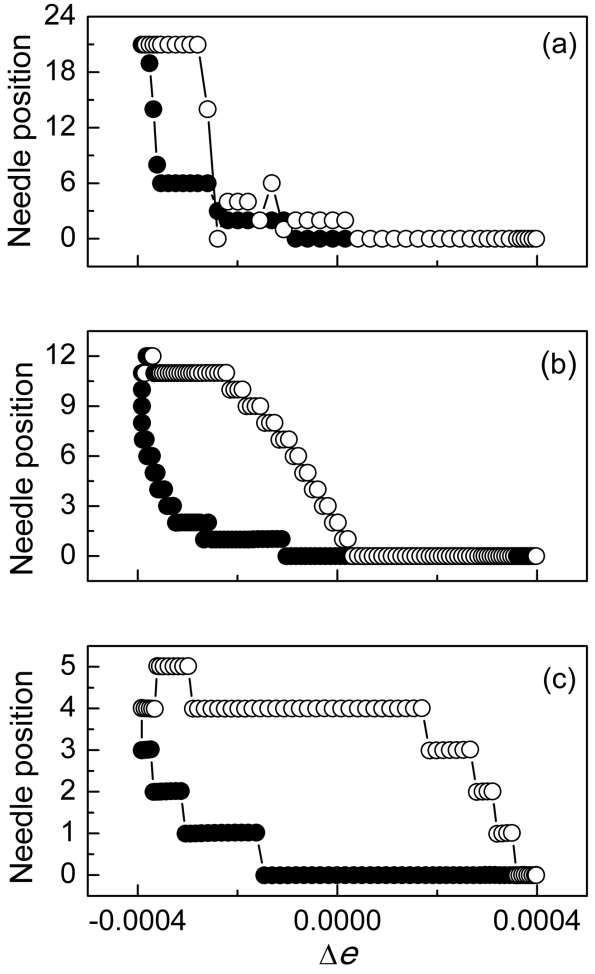

FIGURE 4. Needle position as function of the applied strain for one oscillation of Δe [=A sin (ωt)]. The time period of input sine-wave Δe in **a** is 500 τ_{phonon}, 50 τ_{phonon} in **b**, and 15 τ_{phonon} in **c**. The filled symbols for the data relative to needle position (which is characterized by displacements between needle tip and horizontal twin boundary (blue line in Fig. 2a) corresponding to (Δe) changes from 0.0004 to –0.0004 and open symbols for needle position corresponding to Δe changes from –0.0004 to 0.0004.

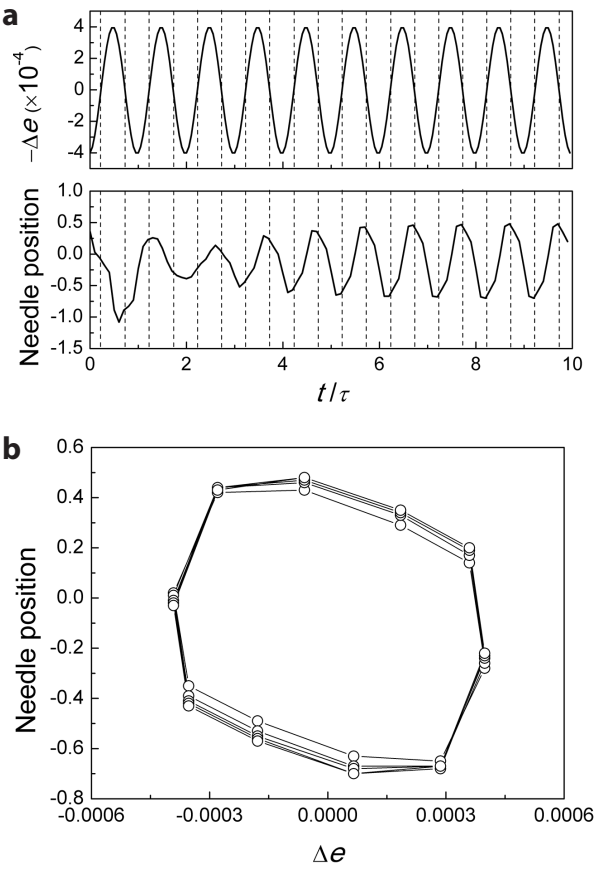

FIGURE 5. (**a**) Applied oscillatory strain Δe [=A sin (ωt)] at the phonon frequency (top) and the position of the needle tip (bottom). After an initial transient pattern, the needle tip vibrates with very low amplitudes (0.5 lattice units) around its stable position. The vibration is phase shifted by π/2 with respect to the applied oscillatory strain. (**b**) Needle position as function of the applied strain for one oscillation at the phonon frequency showing a phase angle of π/2.

the rotation angle is the phase shift φ. Increasing the frequency even further leads to dynamical pinning where the needle tip cannot move within the time of one oscillation of the applied field. The movement by, at least, one lattice unit becomes impossible. The needle tip will then vibrate with the same frequency of the lattice. The movement is now the phonon vibration at the needle tip (Fig. 5), which also shows that the phase factor between the applied oscillated strain (Δe) and phonon frequency is indeed π/2 as expected at the resonance near the phonon frequency. During the forced phonon oscillation we find that the macroscopic stress near the boundary of the external buffer layers and the sample atoms becomes rather large so that new dynamic microstructures appear near the surfaces. The detailed analysis of three layers is beyond the scope of this paper.

Dissipated energy is absorbed by phonons and leads to a heating of the sample. In our MD calculations we usually consider isothermal conditions by connecting the sample to a heat bath. To observe the temperature changes, we disconnected the heat bath from the sample and observed, which geometric change of the microstructure leads to changes of the sample temperature. In Figure 6 three scenarios are shown. We find no temperature change besides the statistical thermal fluctuations when the microstructure does not change (because the driving amplitudes are too low or the frequency is too high). This case is indicated as "purely elastic" in the figure. When the needle is driven strongly and retracts into the upper twin wall, i.e., when the twin wall is topologically destroyed, we find a heat jump, which represents the release of the pinning and self-energy of the needle domain. This event would macroscopically be a large "jerk" as analyzed in Salje et al. (2011a). In the intermediate case, the needle can progress and retract reversibly where each small depinning leads to a heat release followed by a short plateau in which only thermal fluctuations are seen. The repeated retraction and progression of the needle will then heat the sample in an almost continuous fashion. Macroscopically, this case corresponds to friction heating by needle oscillations.

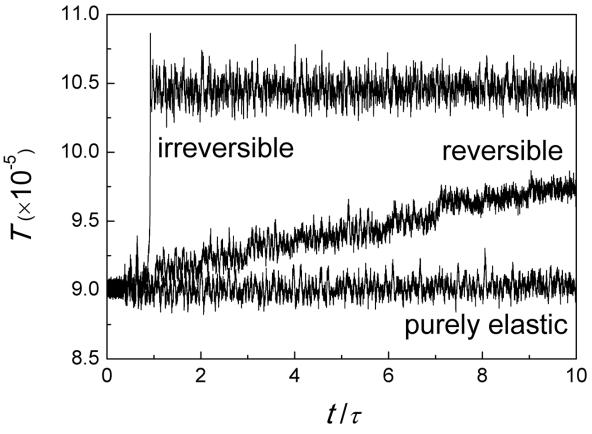

►**Figure 6.** Sample heating by moving needles domains (temperature T in MD units). During the irreversible disappearance of the needle a large temperature jump is seen, which corresponds to a jerk in the energy content of the sample. In purely elastic movements, very little heat is transferred and an almost continuous heating of the sample stems from oscillating needles (in reversible movements).

When the needle retracts beyond a critical distance, the movement becomes irreversible and the needle shrinks critically until it is destroyed (Fig. 7). This effect defines two phases, namely one for the reversible needle retraction and one for the irreversible retraction. The critical needle length defines then the irreversibility line as function of the frequency of the applied oscillatory strain. The applied oscillated strain amplitude (A) at critical line is shown in Figure 8. The amplitude increases with increasing frequency. The physical reason for this frequency dependence is that the needle can follow the strain only at low frequencies while

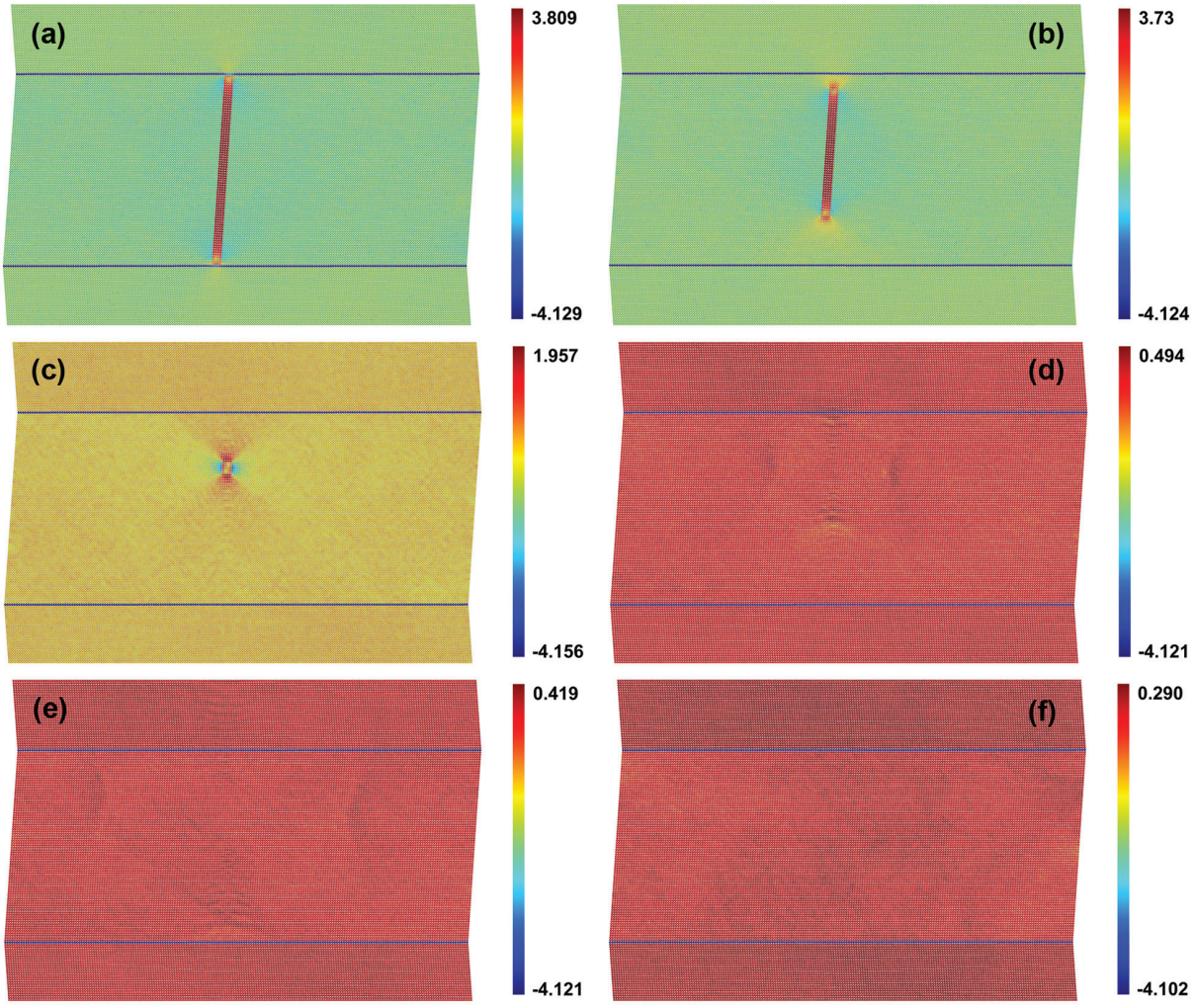

Figure 7. Snapshots of the irreversible retraction of a needle domain under external strain. The needle first detaches initially at the bottom twin boundary (**a**), then at the top boundary (**b**). The total length of the needle then reduces very quickly and disappears in **c**. The strain energy, which was absorbed by the needle is now released into the lattice and leads to changes of the shear angles, which propagate as phonon excitations in **d**–**f**. Ultimately, the sample will relax to the initial shear configuration but without the needle domain. Note that the horizontal twin boundaries (blue lines) do not change their position during the needle collapse.

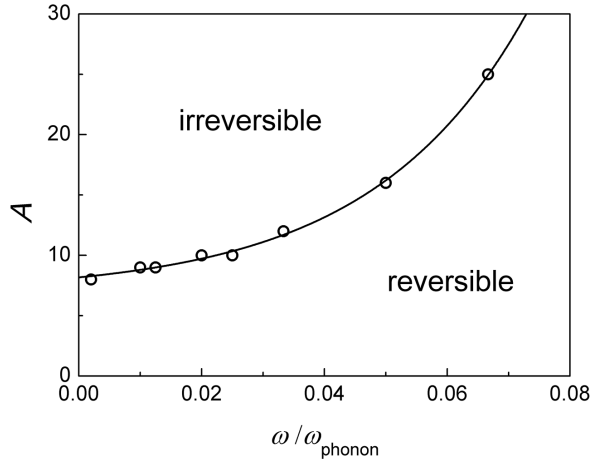

FIGURE 8. Phase diagram of the reversible and irreversible phase as function of the applied oscillatory strain amplitude (A) and frequency. In the reversible phase, the needle will detach and return to the initial position when the field is reversed, in the irreversible phase, the needle domain is destroyed.

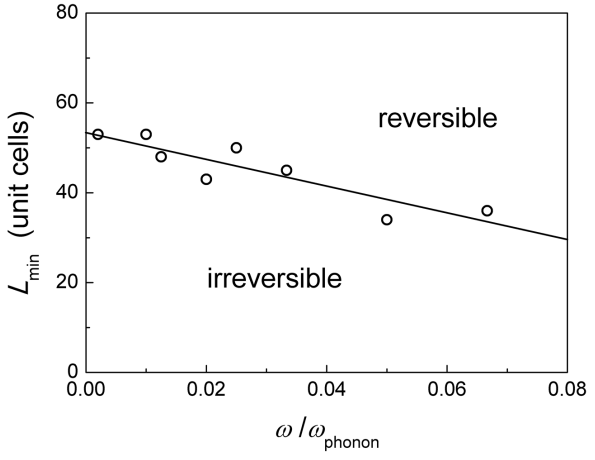

FIGURE 9. Phase boundary between the reversible and irreversible phase shown as function of frequency and the minimum needle length beyond which the needle domain will destruct. The total distance between the anchoring twin walls is 100 lattice lengths, the typical critical needle length is 50 lattice lengths or half the distance between the twin walls.

at high frequencies the needle movement is retarded and cannot follow the external oscillation. If we now consider the needle length itself, we can construct the same phase diagram (Fig. 9) as a function of the needle length vs. frequency. In this parameter space the retardation is eliminated because it only concerns the phase shift between the applied strain and the needle position. We now see that the irreversibility line slightly decreases with increasing frequency. The characteristic critical needle length is 50 lattice units, which is half the distance between the bordering twin walls. This means that the movement becomes irreversible when the needle retracts by half its original length, namely the distance between the bordering twin walls.

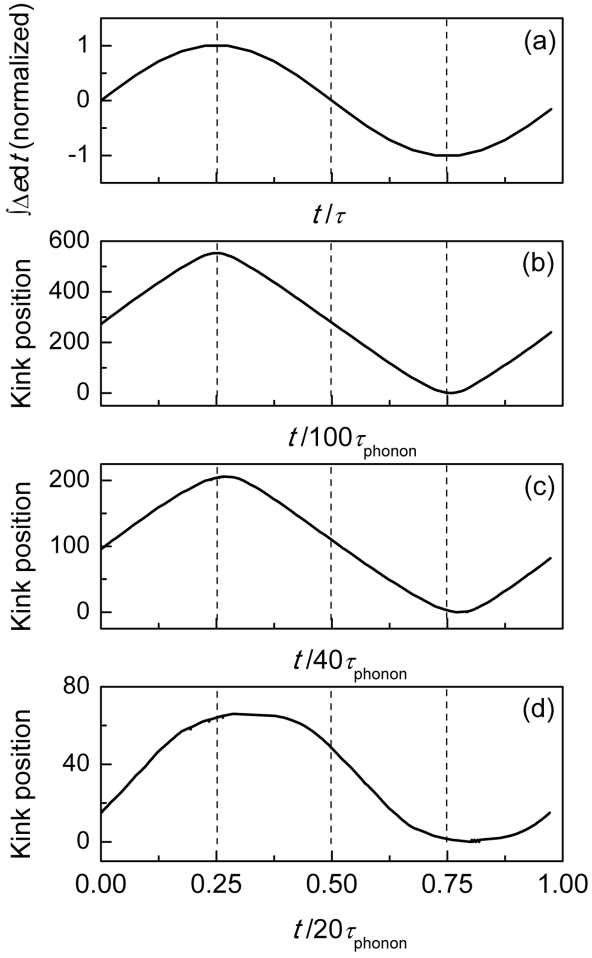

FIGURE 10. Frequency dependence of the kink movement. The driving force (prescribed shear strain) for the kink movement is shown in (**a**), the low-frequency response is in phase with this force (**b**). Increasing frequencies lead to a phase shift of the response function (**c**,**d**).

Kink movement

Kink movements at sufficiently low frequencies are in phase with the applied strain (Fig. 10a). The kink moves over large lattice distances (>100 lattice lengths) with an almost constant speed (Figs. 10b–10c) so that the traditional description of the kink movement as ballistic is indeed correct. The ballistic movement is generated by the internal friction, which, in turn, leads to the heating of the sample (Fig. 2b). When the frequency of the applied force is increased we find the same phase shift as in case of retracting needle domains (Figs. 10c–10d). We find that the kink movement becomes so small that it extends only over 3 unit lengths or less at very high frequencies of 1/5 phonon frequency (Fig. 11b) and at 1/2 phonon frequency (Fig. 11c). The limiting distance reaches one unit length so that kink movements are impossible at zero temperature at the phonon frequency. Some movement is still observed at a finite simulation temperature, which shows all the hallmarks or thermally assisted hopping. Only when the thermal excitation acts in phase with the applied field will a jump occur while no jump is possible otherwise.

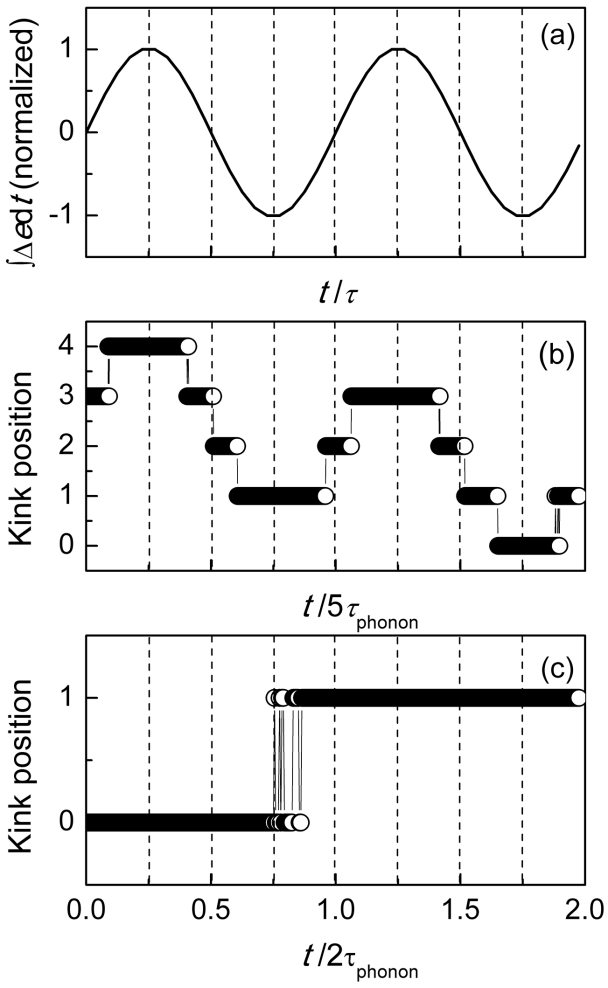

FIGURE 11. High-frequency driving of the kink with very small traveling distances. The frequency is 1/5 ω_{phonon} (**b**) and 1/2 ω_{phonon} (**c**).

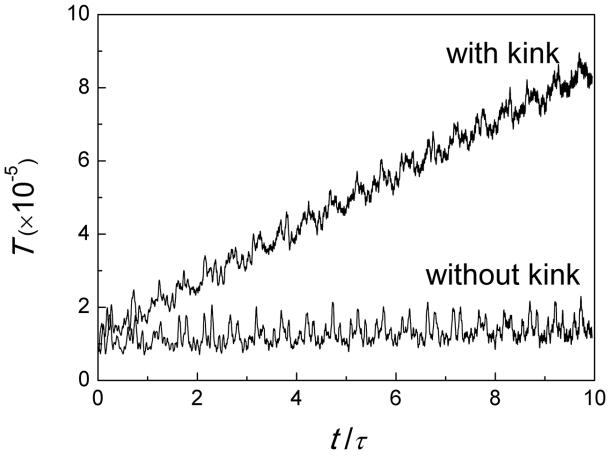

FIGURE 12. Phonon heating by kink progression. The linear increase below the thermal fluctuations represents friction heating. No kink jerks have been observed.

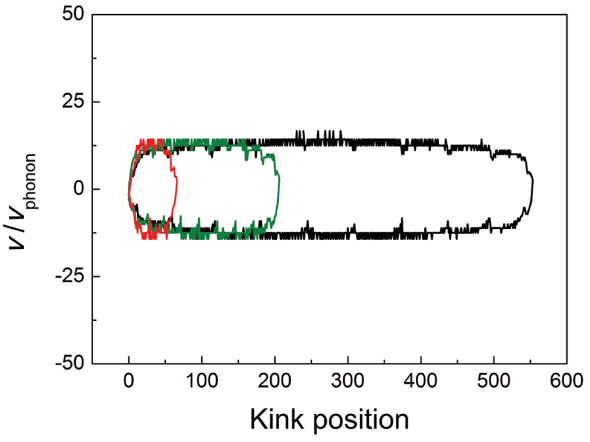

FIGURE 13. Frequency independence of the kink velocity and accelerated movement when the direction of the kink motion is reversed.

The friction movement of the kinks is also seen by the heat transfer from the applied field to the heat bath. When the oscillatory strain is applied without the presence of a moving kink, we find that virtually no heating occurs. When the kink is introduced, it will travel with a constant speed at low frequencies in a friction dominated dynamics. The friction leads to the emission of phonons and hence to the increase of the sample temperature (Fig. 12). The details of the kink motion are shown in Figure 13. The speed of the kink between the endpoints where the direction of the movement is reversed is identical for all applied strain frequencies. The speed of the kink motion is hence an intrinsic feature of the phonon coupling between the moving kink and the attached phonon cloud (Fig. 2b). Increasing or decreasing the frequency of the applied strain does not change the kink velocity. Accelerated movements occur whenever the direction of the movement is reversed. The data in Figure 13 show that the acceleration profile is identical for all applied frequencies so that the way the moving kink reverses its direction is again an intrinsic parameter and does not depend on the external forcing.

DISCUSSION

We have shown that our very simple mechanical model captures the essential results of RUS and DMA. The model contains harmonic springs and two identical Landau springs, which provide the anharmonicity required to generate phase transitions and microstructures. The geometrical microstructures are surprisingly realistic. The dynamical excitations are also well described: the harmonic lattice has only one excitation, namely the acoustic phonons. Below that timescale, much slower processes occur and depend directly on the Landau springs. These excitations relate to changes and vibrations of the microstructure. We have singled out two fundamental excitations: the movement of needle domains and kinks. When these movements expand over large distances compared with the interatomic distances, we find that the typical description of "friction," as overdamped movement in the constant velocity limit, is adequate. This motion leads to heating of the sample.

High-frequency movements are more complicated because the amplitude of the movement is only a few lattice parameters

or even shorter. The shortest distance movements are identified as phonon processes, which do not lead to changes of the microstructure. Slightly larger movements may transfer a needle tip between adjacent or closely spaced lattice points, so that any description in the friction limit becomes wrong. No movement with constant speed can develop because the time provided by the forcing strain movement is simply too short. The damping is hence much less, in agreement with RUS observations.

The needle movement is reversible as long as the needle does not retract beyond the critical value and disappears. This threshold for the irreversible movement is reached in our simulations when the needle retracts by almost half the distance between the two anchoring horizontal twin boundaries. The macroscopic signal for the irreversible movement is a jerk, which would not contribute to the RUS signal. It leads to a heat spike as observed in specific hat measurements. The needle movement is intrinsically irreversible when the needle disappears at the sample surface or when the needle nucleates at a junction, which subsequently disappears when the external strain is reversed. The kink motion has no equivalent irreversibility line as the needle movement, the irreversibility is simply given by the proximity of the kink to the sample surface. We now discuss only topologically stable needle movements for driving forces below the irreversibility threshold.

The total displacement of the needle at moderate frequencies, $\omega << \omega_{phonon}$, consists first of the unpinning and then the retraction. A simple estimate at low frequencies is that the retraction distance D is proportional to the time-period $\tau = 2\pi/\omega$ of an external oscillation with frequency ω. The speed of the needle retraction is then D/τ, which is almost constant in our simulation. The maximum strain is independent of the applied frequency. The total needle movement in the hysteresis DW is also nearly independent of frequency so that the width of the hysteresis becomes $W \sim 1/\tau \sim \omega$. The physical scenario is then the following: after depinning in the stable regime the needle will initially retract with an almost constant speed. When the strain decreases the needle will retract. When the distance D is below one unit cell, no needle movement occurs and the dynamical excitation is entirely phononic.

In RUS experiments we estimated that the needle retraction is ca. 5 unit cells. The phase angle for such short distance movement is near $\pi/2$ in our simulations, which explains the observed phase shifts. The needle will always reverse to the initial position at low frequencies when the relative strain Δe is not too large. If Δe is very large it leads to the irreversible destruction of the needle. This shows that in our model the attractive force between the needle tip and the twin wall is sufficiently large to prevent needles from being metastably stranded at some distance from the twin boundary. This result agrees with earlier calculations, which showed that needle domains are always attracted by orthogonal twin walls (Novak et al. 2002; Lee et al. 2002).

This effect somewhat limits the change of phase angle. In real minerals we often observe needle domains where the needle tip is extrinsically pinned at some distance from the twin wall. This leads to bi-stable movements: the needle tip is either pinned by the twin wall or by the extrinsic defect. The pinning and unpinning dynamics can now occur at any phase angle even at low frequencies. If the depinning occurs at low strains, the strain field and the needle position oscillate in phase. If depinning occurs only at the maximum strain, the phase shift is $\pi/2$. Any other intermediate phase angle depends simply on the pinning strength. These low-frequency phase angles are then modified by the dynamical effects as described above so that the movement of needle domains over small distances can leads to phase shift of RUS signals by virtually any angle.

In summary, we have shown that a simple mechanical model can reproduce the essential findings of mechanical spectroscopy. We have shown which microstructural changes occur over a large frequency range when no defects influence the intrinsic behavior. This does not mean that the sample behaves as a defect free single crystal because the microstructure itself acts as a very complex defect field in which all typical features of pinning and depinning, jerks and surface elimination of kinks occur. In a forthcoming work we will focus on extrinsic defects and ask what role they play when they are added to the intrinsic microstructure.

Acknowledgments

E.K.H.S. is grateful for support by the Leverhulme fund (RG66640) and EPSRC (EP/K009702/1) Z.Z., X.D., and J.S. appreciate the support of NSFC (51171140, 51231008), the 973 Program of China (2010CB631003, 2012CB619402), and 111 project (B06025).

References cited

Baró, J., Corral, A., Illa, X., Planes, A., Salje, E.K.H., Schranz, W., Soto-Parra, D.E., and Vives, E. (2013) Statistical Similarity between the Compression of a porous material and earthquakes. Physical Review Letters, 110, 088702.

Ben-Zion, Y., and Lyakhovsky, V. (2002) Accelerated seismic release and related aspects of seismic pattern on earthquake faults. Pure and Applied Geophysics, 159, 2385–2412.

Born, M., and Huang, K. (1954) Dynamical Theory of Crystal Lattices. Clarendon Press, Oxford, U.K.

Boussinot G., Le Bouar, Y., and Finel A. (2010) Phase-field simulations with inhomogeneous elasticity: Comparison with an atomic-scale method and application to superalloys. Acta Materialia, 58, 41704181.

Calleja, M., Dove, M.T., and Salje, E.K.H. (2003) Trapping of oxygen vacancies on twin walls of $CaTiO_3$: A computer simulation study. Jounal of Physics: Condensed Matter, 15, 2301–2307.

Carpenter, M.A., and Salje, E.K.H. (1998) Elastic anomalies in minerals due to structural phase transitions. European Journal of Mineralogy, 10, 693–812.

Carpenter, M.A., Li, B., and Liebermann, R.C. (2007) Elastic anomalies accompanying phase transitions in $(Ca,Sr)TiO_3$ perovskites: Part III. Experimental investigation of polycrystalline samples. American Mineralogist, 92, 344–355.

Daraktchiev, M., Salje, E.K.H., Lee, W.T., and Redfern, S.A.T. (2007) Effect of internal friction on transformation twin dynamics in perovskite $Sr_xBa_{1-x}SnO_3$ ($x = 0.6, 0.8$). Physical Review B, 75, 134102.

Deng, J.K., Ding, X.D., Lookman, T., Suzuki, T., Otsuka, K., Sun, J., Saxena, A., and Ren, X. (2010) Microscopic mechanism of martensitic stabilization in shape-memory alloys: Atomic-level processes. Physical Review B, 81, 220101.

Ding, X.D., Suzuki, T., Ren, X.B., Sun, J., and Otsuka, K. (2006) Precursors to stress-induced martensitic transformations and associated superelasticity: Molecular dynamics simulations and an analytical theory. Physical Review B, 74, 104111.

Ding, X., Zhao, Z., Lookman, T., Saxena, A., and Salje, E.K.H. (2012) high junction and twin boundary densities in driven dynamical systems. Advanced Materials, 24, 5385–5389.

Froseth, A., Van Swygenhoven, H., and Derlet, P.M. (2004) The influence of twins on the mechanical properties of nc-Al. Acta Materialia, 52, 2259–2268.

Gallardo, M.C., Manchado, J., Romero, F.J., del Cerro, J., Salje, E.K.H., Planes, A., Vives, E., Romero, R., and Stipcich, M. (2010) Avalanche criticality in the martensitic transition of $Cu_{67.64}Zn_{16.71}Al_{15.65}$ shape-memory alloy: A calorimetric and acoustic emission study. Physical Review B, 81, 174102.

Goncalves-Ferreira, L., Redfern, S.A.T., Atacho, E., and Salje, E.K.H. (2009) The intrinsic elasticity of twin walls: Ferrielectric twin walls in ferroelastic $CaTiO_3$. Applied Physics Letters, 94, 081903.

Groger, R., Lookman, T., and Saxena, A. (2008) Defect-induced incompatibility of elastic strains: Dislocations within the Landau theory of martensitic phase transformations. Physical Review B, 78, 184101.

Harrison, R.J., Redfern, S.A.T., and Street, J. (2003) The effect of transformation twins on the seismic-frequency mechanical properties of polycrystalline $Ca_{1-x}Sr_xTiO_3$ perovskite. American Mineralogist, 88, 574–582.

Harrison, R.J., Redfern, S.A.T., and Salje, E.K.H. (2004a) Dynamical excitation and anelastic relaxation of ferroelastic domain walls in $LaAlO_3$. Physical

Review B, 69, 144101.
Harrison, R.J., Redfern, S.A.T., Buckley, A., and Salje, E.K.H. (2004b) Application of real-time, stroboscopic X-ray diffraction with dynamical mechanical analysis to characterize the motion of ferroelastic domain walls. Journal of Applied Physics, 95, 1706–1717.
Hashin, Z., and Shtrikman, S. (1963) A variational approach to the theory of the elastic behaviour of multiphase materials. Journal of the Mechanics and Physics of Solids, 11, 127–140.
Haussuehl, S. (1960) Thermo-elastische Konstanten der Alkalihalogenide vom NaCl-typ. Zeitschrift fuer Physik, 159, 223–229.
Isaak, D.G., and Ohno, I. (2003) Elastic constants of chrome-diopside: Application of resonant ultrasound spectroscopy to monoclinic single-crystals. Physics and Chemistry of Minerals, 30, 430–439.
Isaak, D.G., Ohno, I., and Lee, P.C. (2006) The elastic constants of monoclinic single-crystal chrome-diopside to 1300 K. Physis and Chemistry of Minerals, 32, 691–699.
Jackson, I., Faul, U.F., FitzGerald, J.D., and Morris, S.J.S. (2006) Contrasting viscoelastic behaviour of melt-free and melt-bearing olivine: implications for the nature of grain-boundary sliding. Materials Science and Engineering, A, 442, 170–174.
Jackson, I., Barnhoorn, A., Aizawa, Y., and Saint, C. (2009) Improved procedures for the laboratory study of high-temperature viscoelastic relaxation. Physics of the Earth and Planetary Interiors, 172, 104–115.
Jacobs, E. (2000) Landau theory of structures in tetragonal-orthorhombic ferroelastics. Physical Review B, 61, 6587.
Kachaturynan, A.G. (2008) Theory of Structural Transformations in Solids. Wiley, New York.
Kityk, A.V., Schranz, W., Sondergeld, P., Havlik, D., Salje, E.K.H., and Scott, J.F. (2000) Low frequency superelasticity and nonlinear elastic behaviour of SrTiO3 crystals. Physical Review B, 61, 946.
Kremer, F., and Schonhals, A. (2002) Broadband Dielectric Spectroscopy. Springer, Berlin.
Lee, P.C.Y., Liu, N.H., and Ballato, A. (2004) Thickness vibrations of a piezoelectric plate with dispersion. IEEE Transactions on Ultrasonics Ferroelectrics and Frequency Control, 51, 52–62.
Lee, W.T., Salje, E.K.H., and Bismayer, U. (2002) Surface structure of domain walls in a ferroelastic system with a domain wall pressure. Journal of Physics: Condensed Matter, 14, 7901–7910.
Lee, W.T., Salje, E.K.H., Goncalves-Ferreira, L., Daraktchiev, M., and Bismayer, U. (2006) Intrinsic activation energy for twin-wall motion in the ferroelastic perovskite $CaTiO_3$. Physical Review B, 73, 214110.
McKnight, R.E.A., Carpenter, M.A., Darling, T.W., Buckley, A., and Taylor, P.A. (2007) Acoustic dissipation associated with phase transitions in lawsonite, $CaAl_2Si_2O_7(OH)_2H_2O$. American Mineralogist, 92, 1665–1672.
Mehta, A.P., Mills, A.C., Dahmen, K.A., and Sethna, J.P. (2002) Universal pulse shape scaling function and exponents: Critical test for avalanche models applied to Barkhausen noise. Physical Review, E, 65, 046139.
Migliori, A., and Maynard, J.D. (2005) Implementation of a modern resonant ultrasound spectroscopy system for the measurement of the elastic moduli of small solid specimens. Review of Scientific Instruments, 76, 121301.
Milton, G.W. (2002) The Theory of Composites. Cambridge University Press, U.K.
Morris, S.J.S., and Jackson, I. (2009) Diffusionally assisted grain-boundary sliding and viscoelasticity of polycrystals. Journal of the Mechanics and Physics of Solids, 57, 744–761.
Novak, J., Bismayer, U., and Salje, E.K.H. (2002) Simulated equilibrium shapes of ferroelastic needle domains. Journal of Physics: Condensed Matter, 14, 657–664.
Ohno, I., Abe, M., Kimura, M., Hanayama, Y., Oda, H., and Suzuki, I. (2000) Elasticity measurement of silica glass under gas pressure. American Mineralogist, 85, 288–291.
Parlinski, K., Salje, E.K.H., and Heine, V. (1993) Annealing of tweed microstructure in high *T*c superconductors studied by a computer simulation. Acta Metallurgica et Materialia, 41, 839–847.
Perez-Reche, F.J., Tadic, B., Manosa, L., Planes, A., and Vives, E. (2004) Driving rate effects in avalanche-mediated first-order phase transitions. Physical Review Letters, 93, 195701.
Prencipe, M., Noel, Y., Bruno, M., and Dovesi, R. (2009) The vibrational spectrum of lizardite-1*T* $[Mg_3Si_2O_5(OH)_4]$ at the Γ point: A contribution from an ab initio periodic B3LYP calculation. American Mineralogist, 94, 986–994.
Romero, F.J., Manchado, J., Martin-Olalla, J.M., Gallardo, M.C., and Salje, E.K.H. (2011) Dynamic heat flux experiments in $Cu_{67.64}Zn_{16.71}Al_{15.65}$: Separating the timescales of fast and ultra-slow kinetic processes in martensitic transformations. Applied Physics Letters, 99, 011906.
Salje, E.K.H. (2007) An empirical scaling model for averaging elastic properties including interfacial effects. American Mineralogist, 92, 429–432.
——— (2008) (An)elastic softening from static grain boundaries and possible effects on seismic wave propagation. Physics and Chemistry of Minerals, 35, 321–330.
——— (2010) Multiferroic boundaries as active memory devices: Trajectories towards domain boundary engineering. ChemPhysChem, 11, 940–950.
——— (2012) Ferroelastic materials. Annual Review of Materials Research, 42, 265–283.
Salje, E.K.H., and Carpenter, M.A. (2011) High frequency elastic losses in $LaAlO_3$ and its importance for $LaAlO_3/SrTiO_3$ heterojunctions. Applied Physics Letters, 99, 051907.
Salje, E., and Parlinski, K. (1991) Microstructures in high Tc superconductors. Superconductor Science and Technology, 4, 93–97.
Salje, E.K.H., and Schranz, W. (2011) Low amplitude, low frequency elastic measurements using dynamic mechanical analyzer (DMA) spectroscopy. Zeitschrift für Kristallographie, 226, 1–17.
Salje, E., and Zhang, H.L. (2009a) Domain boundary engineering. Phase Transitions, 82, 452–469.
——— (2009b) Domain boundary pinning and elastic softening in $KMnF_3$ and $KMn_{1-x}Ca_xF_3$. Journal of Physics: Condensed Matter, 21, 035901.
Salje, E., Palosz, B., and Wruck, B. (1987) In situ observation of the polytypic phase transition 2H-12R in PbI2: investigations of the thermodynamic structural and dielectric properties. Journal of Physics: Condensed Matter, 20, 4077–4087.
Salje, E.K.H., Koppensteiner, J., Reinecker, M., Schranz, W., and Planes, A. (2009) Jerky elasticity: Avalanches and the martensitic transition in $Cu_{74.08}Al_{23.13}Be_{2.79}$ shape-memory alloy. Applied Physics Letters, 95, 231908.
Salje, E.K.H., Ding, X., Zhao, Z., Lookman, T., and Saxena, A. (2011a) Thermally activated avalanches: Jamming and the progression of needle domains. Physical Review B, 83, 104109.
Salje, E.K.H., Enrique Soto-Parra, D., Planes, A., Vives, E., Reinecker, M., and Schranz, W. (2011b) Failure mechanism in porous materials under compression: crackling noise in mesoporous SiO_2. Philosophical Magazine Letters, 91, 554–560.
Salje, E.K.H., Safarik, D.J., Lashley, J.C., Groat, L.A., and Bismayer, U. (2011c) Elastic softening of metamict titanite $CaTiSiO_5$: Radiation damage and annealing. American Mineralogist, 96, 1254–1261.
Salje, E.K.H., Ding, X., Zhao, Z., and Lookman, T. (2012) How to generate high twin densities in nano-ferroics: Thermal quench and low temperature shear. Applied Physics Letters, 100, 222905.
Salje, E.K.H., Lampronti, G.I., Soto-Parra, D.I., Baró, J., Planes, A., and Vives, E. (2013) Noise of collapsing minerals: Predictability of the compressional failure in Goethite mines. American Mineralogist, 98, 609–615.
Schranz, W., Sondergeld, P., Kityk, A.V., and Salje, E.K.H. (2009) Dynamic elastic response of $KMn_{1-x}Ca_xF_3$: Elastic softening and domain freezing. Physical Review B, 80, 094110.
Schroder, H., Samwer, K., and Koster, U. (1985) Micromechanics for metallic-glass formation by solid state reactions. Physical Review Letters, 54, 197–200.
Scott, J.F., Salje, E.K.H., and Carpenter, M.A. (2012) Domain wall damping and elastic softening in $SrTiO_3$: evidence for polar twin walls. Physical Review Letters, 109, 187601.
Sethna, J.P., Dahmen, K.A., and Myers, C.R. (2001) Crackling noise. Nature, 410, 242–250.
Spasojevic, D., Bukvic, S., Milosevic, S., and Stanley, H.E. (1996) Barkhausen noise: Elementary signals, power laws, and scaling relations. Physical Review, E, 54, 2531–2546.
Van Aert, S., Turner, S., Delville, R., Schryvers, D., Van Tendeloo, G., and Salje, E.K.H. (2012) Direct observation of ferrielectricity at ferroelastic domain boundaries in $CaTiO_3$ by electron microscopy. Advanched Materials, 24, 523–527.
Vives, E., and Planes, A. (1994) Avalanches in a fluctuationless 1st-order phase transition in a random-bond Ising-model. Physical Review B, 50, 3839–3848.
Vives, E., Soto-Parra, D., Planes, A., Manosa, L., Romero, R., and Edwards, R. (2011) Acoustic emission avalanches in martensitic transitions: new perspectives for the problem of source location. Diffusion and Defect Data Part B (Solid State Phenomena), 172–174, 144–149.
Zhang, Z., Koppensteiner, J., Schranz, W., and Carpenter, M.A. (2012a) Elastic and anelastic anomalies due to spin-state transitions in orthorhombic perovskite from isoelectronic behavior of Co^{3+} and Fe^{2+}. American Mineralogist, 97, 1714–1725.
——— (2012b) Variations in elastic and anelastic properties of Co_3O_4 due to magnetic and spin-state transitions. American Mineralogist, 97, 399–406.

Manuscript received December 5, 2012
Manuscript accepted April 16, 2013
Manuscript handled by Sergio Speziale